

Liquid-Liquid Critical Point in Phosphorus

Manyi Yang¹, Tarak Karmakar¹, and Michele Parrinello^{1*}
Italian Institute of Technology, Via Melen 83, 16152 Genova, Italy

 (Received 4 May 2021; revised 7 July 2021; accepted 19 July 2021; published 17 August 2021)

The study of liquid-liquid phase transitions has attracted considerable attention. One interesting example of this phenomenon is phosphorus, for which the existence of a first-order phase transition between a low density insulating molecular phase and a conducting polymeric phase has been experimentally established. In this Letter, we model this transition by an *ab initio* quality molecular dynamics simulation and explore a large portion of the liquid section of the phase diagram. We draw the liquid-liquid coexistence curve and determine that it terminates into a second-order critical point. Close to the critical point, large coupled structure and electronic structure fluctuations are observed.

DOI: [10.1103/PhysRevLett.127.080603](https://doi.org/10.1103/PhysRevLett.127.080603)

One phenomenon that has attracted much attention is that of liquid-liquid (LL) phase transitions. Most famously, the existence of such an LL transition terminating in a critical point has been suggested as a possible explanation for the famous water anomalies [1–9]. Unfortunately the location of this transition in the so-called “no man’s land” has made its experimental study challenging. Besides water, the existence of LL transitions has been discussed in a number of other systems [10–17]. However, experimental investigations in these systems are also fraught with difficulties since the reported LL transitions occur in a regime of high temperatures and pressures.

Among the many systems for which an LL transition has been reported, the most intriguing example is that of liquid phosphorus. Phosphorus is an interesting substance with several practical applications, and already, in the solid phase, it exhibits many allotropes. Thus, it is perhaps not a surprise that different structures can also be found in the liquid state. Katayama *et al.* [18,19] have reported experimental evidence of the existence of a first-order LL transition as signaled by an abrupt density jump. The low-density liquid (LDL) phase is an insulating fluid whose structural units are P_4 molecules, while the high-density liquid (HDL) phase is a conducting fluid whose structure has been described as polymeric. Subsequent experiments have revealed that the slope of the LL transition line in the temperature-pressure (TP) plane is negative [20]. In addition, the existence of a liquid-liquid critical point at $T \geq 2500$ K has been conjectured but so far no firm experimental evidence has been reported.

This obviously calls for simulations that can clarify the behavior of liquid phosphorus and, in particular, the existence of a critical point. This task is made difficult by the metal to nonmetal transition that accompanies the LL transition. The change in chemical bonding renders a standard approach to the development of a realistic phosphorus force field challenging. A possible alternative is to

use *ab initio* molecular dynamics simulations in which the forces are computed on the fly from accurate electronic structure calculations. Typically, the forces are calculated by using density functional theory (DFT), which provides a balance between computational expediency and accuracy. A number of such simulations have been reported, and they all have shown that a DFT-based approach is able to reproduce the existence of the LL transition [21–24]. A somewhat indirect attempt has also been made at estimating the critical point [25,26]. Although these simulations are highly illuminating, their computational cost has required some compromise as to the system size and the simulation length and has allowed only for a limited number of thermodynamics states to be explored.

A way of obtaining *ab initio* MD accuracy at a limited computational cost was suggested some time ago by Behler and Parrinello [27,28]. Their idea was to use the generalization capabilities of neural networks (NN) to express the potential energy surface. The parameters of the NN were trained on a relatively large set of DFT calculations performed on appropriately selected atomic configurations. Since Behler and Parrinello’s work, much progress has been made, and their approach has become very popular [29–35]. Here, we shall use, as we have done in the recent past [36–38], the Deep MD code [39,40]. In the case of phosphorus, an approach similar in spirit but based on the Gaussian Kernel representation of the potential has already been used to study its allotropes and liquid state [41]. However, the exploration of the high pressure and high temperature part of the phase diagram has been limited.

In the Behler-Parrinello-type approach, a judicious choice of the training configurations is important. In our case, the choice of configurations is complicated by the fact that a first-order phase transition is a rare event. Therefore, the transition state configurations that are essential for determining the transition barrier between one phase and the other are rarely sampled and are not encoded in the NN.

For this reason, when studying rare events, we have proposed to train the NN extracting configurations from an enhanced sampling run where the low probability but highly important transition state arrangements are sampled [36–38]. Furthermore, in the study of phase diagrams, it is convenient to follow Refs. [37] and [42,43] and use a multithermal multibaric (MultiTP) enhanced sampling method. The MultiTP approach allows entire regions of the TP phase diagram to be explored at a computational cost comparable to that of a single standard simulation at a given temperature and pressure. A full description of the technical details can be found in the Supplemental Material (SM) [44]. Here, we mention only the fact that we use the on-the-fly probability enhanced sampling (OPES) version of the MultiTP approach [61,62]. OPES, like many other enhanced sampling methods [63–65], relies on the definition of a collective variable (CV) whose fluctuations are enhanced by the method [62,66]. A natural choice would have been to use the density as a CV that is the natural order parameter for the phase transition. However, since this CV performed poorly due to its inability to describe the local molecular arrangement, we choose instead the value of the first peak of the Debye structure factor [67] that has contrasting intensity in the LDL and HDL phases (see Fig. S2 in SM [44]). However, we express our results as a function of the density that is a standard thermodynamic variable.

[38,68,69]. That is, one first performs a number of standard *ab initio* MD calculations in a grid of thermodynamic conditions. These configurations are used to obtain a first guess of the NN potential. In reality, four slightly different NN models are obtained by starting the NN stochastic optimization of the NN from different initial conditions. One of these models is then used to drive the MultiTP-OPES calculation. Periodically, we check whether all four NN models predict similar forces. If the discrepancy between their predictions exceeds a preassigned threshold (see the SM [44]), we calculate the DFT energies and forces for those particular configurations and add these data to the training set and at a fixed interval retrain all four NN models. This procedure is continued until no significant discrepancy between the four models is observed. The calculations presented here are based on the SCAN + D3 exchange-correlation model that gives a good agreement between experiment [20] and theory (see Fig. S7 in SM [44]).

Since our MD calculations are based on a MultiTP approach, by following a reweighing technique discussed in Ref. [66] we can calculate the system properties in the range of temperatures and pressures that is specified at the beginning of the calculation without having to perform new simulations. Thus, it is painless to identify the transition line and other significant thermodynamic points. The procedure used to draw the coexistence line is illustrated with the example of the free energy surface behavior as a

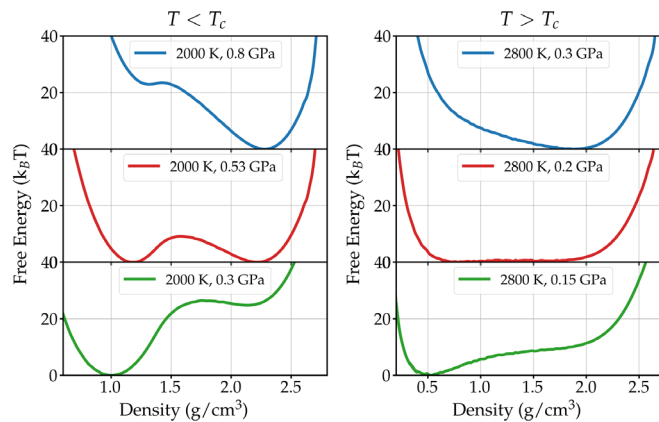


FIG. 1. Free energy surfaces as a function of the density for $T = 2000$ K ($T < T_c$) (left) and $T = 2800$ K ($T > T_c$) (right). For each T , three free energy surfaces at different P values are shown. Error bars, calculated using the weighted block average technique (number of blocks = 4) discussed in Ref. [62], are smaller than the linewidth.

function of pressure at $T = 2000$ K (see Fig. 1, left). At the lower pressure, the LDL phase is more likely, while at the high pressure HDL prevails. The location at which they are equally probable defines the pressure where the two liquids coexist at the selected temperature. This behavior is consistent with a first-order transition, and the locus of such coexistence points defines the boundary line between the two phases.

This behavior is to be contrasted with that at $T = 2800$ K, where pressure induces a continuous change from a LDL-like to an HDL-like structure (see Fig. 1, right). In this region of the phase diagram, one is above the critical point. However, also in this part of the phase diagram, a thermodynamically significant line can be drawn. This is the so called Widom line that can be defined as the locus of a point where properties such as isothermal compressibility, correlation length, and isobaric heat capacity are the highest. Here, we calculated the maximum of the compressibility to draw the Widom line in Fig. 2. At $T = 2800$ K, this point occurs at $P = 0.2$ GPa as a consequence of the fact that the free energy surface curvature is very low, and, therefore, the compressibility is large.

This analysis can be repeated at all desired temperatures and pressures in the preassigned MultiTP range and leads to the phase diagram in Fig. 2. In agreement with experiments [20], the coexistence line has a negative slope. It can be clearly seen that there is a density jump across the phase transition line. As the system approaches the critical point (whose position will be determined below), the jump eventually vanishes. In the same picture we also show two typical structural units of LDL and HDL. In LDL, the structural units are P_4 molecules while the HDL phase is characterized by the presence of small irregular branched multimers of different sizes that continuously form and

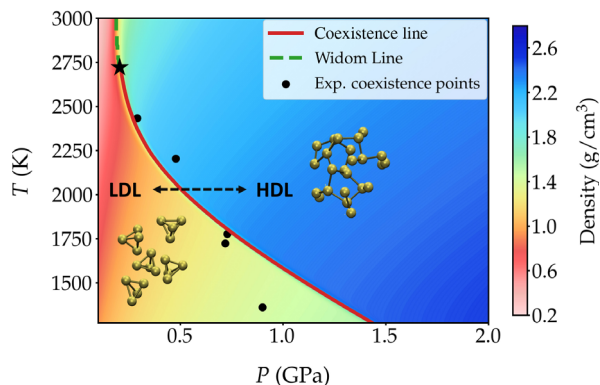


FIG. 2. Liquid phosphorus phase diagram. The value of the density as a function of T and P is also plotted. The LL coexistence line is the red line. Black points denote the experimental coexistence points [20]. The calculated LL critical point is indicated by the black star, and the Widom line (discussed also in Sec. S4.1 in the SM [44]) is shown as a dashed green line. Typical structures of the molecular and polymeric phases are depicted as balls and sticks.

break. One such multimer is shown in the picture. As we approach the critical point from the LDL side we see (see Fig. S10 in SM [44]) that more and more P_4 units are broken. This is to be contrasted with what happens on the HDL side where the multimeric structure is maintained until one gets rather close to the critical point.

We now focus on the transition region. To this effect, we show in Fig. 3 the free energy profiles' evolution along the coexistence curve. At the lower temperatures, the LDL and HDL minima are well separated, reflecting the presence of a first-order transition. However, as the temperature is increased, the barrier between the two phases vanishes and

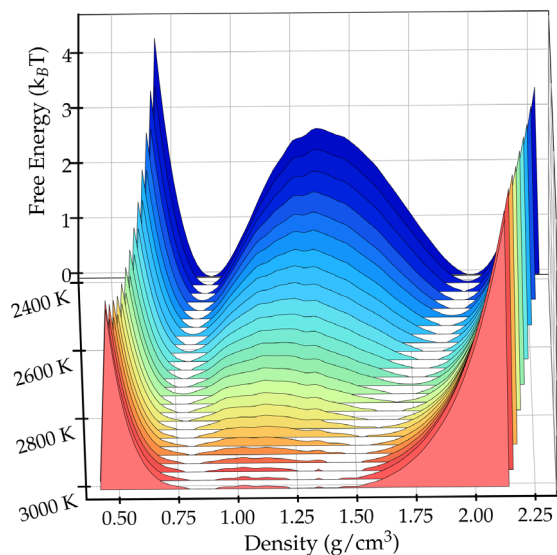


FIG. 3. Free energy surfaces as a function of the density and temperatures along the coexistence line. The color of the free energy surfaces varies from blue at $T = 2400$ K to red at $T = 3000$ K.

the two phases can no longer be distinguished. The barrierless transition between the two regimes identifies the critical point. However, reading its precise position from Fig. 3 is difficult, and in addition one expects large finite size effects. For this reason, we made a Binder cumulant analysis (see Sec. S4.2 in SM [44]) [70,71] that allows us to compute the thermodynamic value of the critical point. In such a way, we estimate for the critical temperature and pressure the values $T_c \sim 2690$ K and $P_c \sim 0.2$ GPa (see Fig. S8 in the SM [44]), which are in line with the indirect ones suggested by the experimentalists [20].

It is fascinating to study the evolution of the electronic structure as reflected in the electronic density of states (DOS) and the inverse participation ratio that provides the extent of localization of electronic states (see Sec. S4.3 in the SM [44] for a detailed discussion). We perform this analysis by computing the electronic structure on selected configurations along the coexistence line.

Deep into the two-phase region, the LDL DOS clearly shows a gap (see Fig. 4, top), and the occupied states are well localized as is to be expected from a molecular liquid. In contrast, the HDL DOS has a metallic character (see Fig. 4, bottom), and the electronic states are rather delocalized (see the SM [44]). The behavior of the LDL as it approaches T_c is rather intriguing since localized states appear in the band gap. These states are localized on the partially broken P_4 molecules (Fig. 5); thus, they will not contribute to a metal type conductivity. As we further approach T_c , the number of broken P_4 molecules increases (see Fig. S10 in the SM [44]) and so does the number of states in the band gap. Right at T_c , as shown in Fig. 6, the

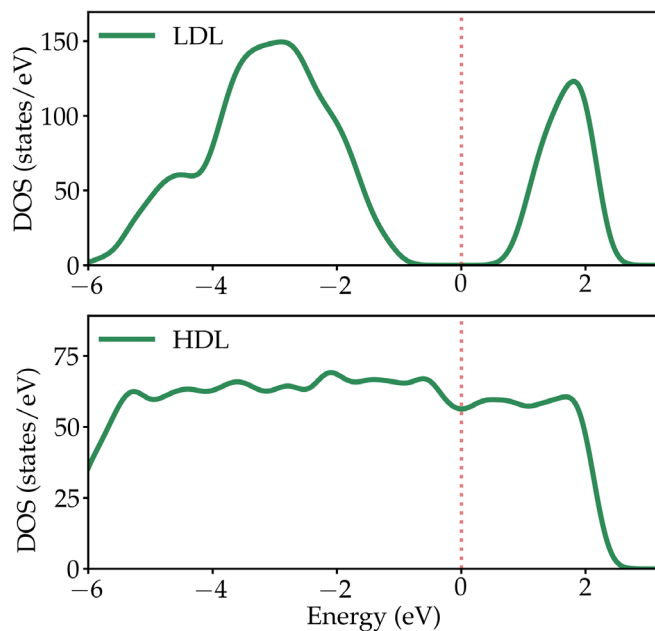


FIG. 4. DOS for configurations in the LDL (top) and HDL (bottom) phase at $T = 1275$ K. The Fermi level is shown as a red dashed line.

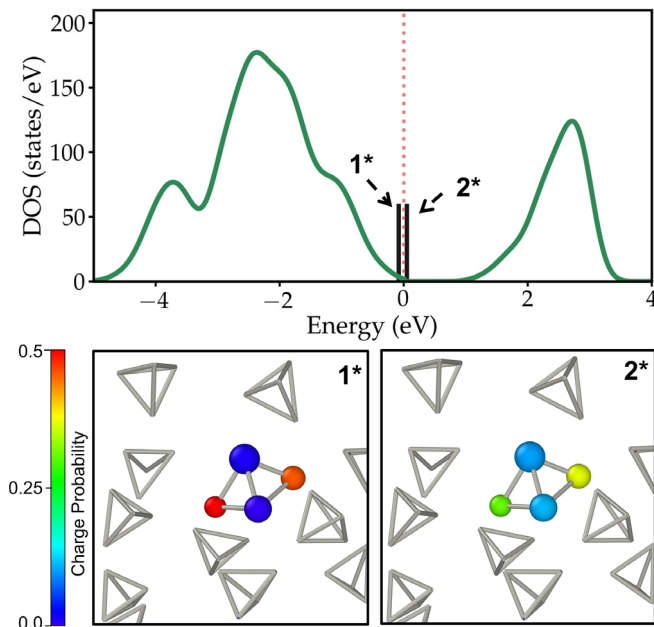


FIG. 5. Top: DOS of a defective LDL configuration. The state 1^* and 2^* are localized on a P_4 molecule in which one of the bonds is broken. The Fermi level is shown as a red dashed line. The probability density on the unbroken P_4 , represented by a stick only, is negligible, while it is significantly large on the broken P_4 , which is represented by (bottom) balls and sticks.

electronic structure undergoes huge fluctuations and goes from a metallic-like character (#1) to an insulator one (#4), passing *via* intermediate states (#2 and #3) such as those described above.

Finally, we hope that this fascinating behavior can be experimentally probed since this is an unusual critical system in which a metal-nonmetal transition is strongly

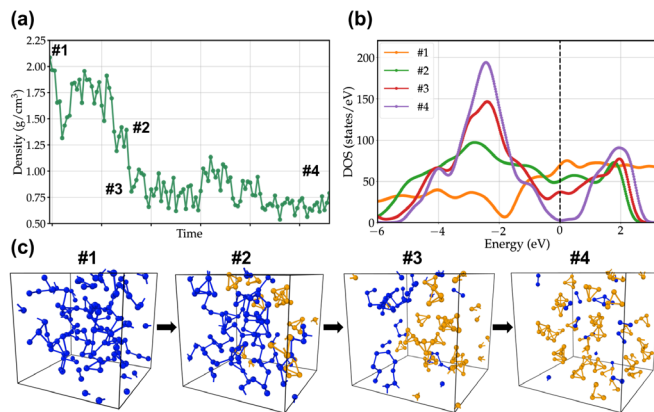


FIG. 6. (a) Density as a function of the simulation time extracted from an unbiased NPT simulation (see Fig. S11 in the SM [44]) run at the critical region ($T = 2700$ K and $P = 0.2$ GPa). The evolution of (b) DOS and (c) structures as the system transits from the polymeric (#1) to the molecular phase (#4). Atoms belonging to polymers are shown in blue, while those belonging to the P_4 units are displayed in yellow.

coupled to a structural one. The success of our strategy that combines MultiTP-OPES with machine learning encourages us to study in the future even more complex systems.

We thank Michele Invernizzi, Chang Woo Myung, Luigi Bonati, and Omar Abou El Kheir for their help and the many useful discussions. The research was supported by the European Union Grant No. ERC-2014-AdG-670227/VARMET. We also thank the NCCR MARVEL, funded by the Swiss National Science Foundation. The computational resources were obtained from the ETH Zurich Euler supercomputer. Part of this work was conducted while the authors were still affiliated to ETHZ and USI, whose support is acknowledged.

*Corresponding author.

michele.parrinello@iit.it

- [1] P. H. Poole, F. Sciortino, U. Essmann, and H. E. Stanley, Phase behaviour of metastable water, *Nature (London)* **360**, 324 (1992).
- [2] F. Sciortino, P. H. Poole, U. Essmann, and H. E. Stanley, Line of compressibility maxima in the phase diagram of supercooled water, *Phys. Rev. E* **55**, 727 (1997).
- [3] L. Xu and V. Molinero, Is there a liquid-liquid transition in confined water?, *J. Phys. Chem. B* **115**, 14210 (2011).
- [4] J. C. Palmer, F. Martelli, Y. Liu, R. Car, A. Z. Panagiotopoulos, and P. G. Debenedetti, Metastable liquid-liquid transition in a molecular model of water, *Nature (London)* **510**, 385 (2014).
- [5] F. Smallenburg and F. Sciortino, Tuning the Liquid-Liquid Transition by Modulating the Hydrogen-Bond Angular Flexibility in a Model for Water, *Phys. Rev. Lett.* **115**, 015701 (2015).
- [6] P. H. Poole, R. K. Bowles, I. Saika-Voivod, and F. Sciortino, Free energy surface of ST2 water near the liquid-liquid phase transition, *J. Chem. Phys.* **138**, 034505 (2013).
- [7] T. E. Gartner, L. Zhang, P. M. Piaggi, R. Car, A. Z. Panagiotopoulos, and P. G. Debenedetti, Signatures of a liquid-liquid transition in an ab-initio deep neural network model for water, *Proc. Natl. Acad. Sci. U.S.A.* **117**, 26040 (2020).
- [8] J. L. Abascal and C. Vega, Widom line and the liquid-liquid critical point for the TIP4P/2005 water model, *J. Chem. Phys.* **133**, 234502 (2010).
- [9] P. G. Debenedetti, F. Sciortino, and G. H. Zerbe, Second critical point in two realistic models of water, *Science* **369**, 289 (2020).
- [10] N. Jakse and A. Pasturel, Liquid-Liquid Phase Transformation in Silicon: Evidence from First-Principles Molecular Dynamics Simulations, *Phys. Rev. Lett.* **99**, 205702 (2007).
- [11] V. V. Vasisht, S. Saw, and S. Sastry, Liquid-liquid critical point in supercooled silicon, *Nat. Phys.* **7**, 549 (2011).
- [12] V. Dzhabura, M. Zaghoo, and I. F. Silvera, Evidence of a liquid-liquid phase transition in hot dense hydrogen, *Proc. Natl. Acad. Sci. U.S.A.* **110**, 8040 (2013).
- [13] E. Lascaris, Tunable Liquid-Liquid Critical Point in an Ionic Model of Silica, *Phys. Rev. Lett.* **116**, 125701 (2016).

- [14] R. Kurita and H. Tanaka, Critical-like phenomena associated with liquid-liquid transition in a molecular liquid, *Science* **306**, 845 (2004).
- [15] R. Kurita and H. Tanaka, On the abundance and general nature of the liquid-liquid phase transition in molecular systems, *J. Phys. Condens. Matter* **17**, L293 (2005).
- [16] M. Huš and T. Urbic, Existence of a liquid-liquid phase transition in methanol, *Phys. Rev. E* **90**, 062306 (2014).
- [17] M. W. C. Dharma-Wardana, D. D. Klug, and R. C. Remsing, Liquid-Liquid Phase Transitions in Silicon, *Phys. Rev. Lett.* **125**, 075702 (2020).
- [18] Y. Katayama, T. Mizutani, W. Utsumi, O. Shimomura, M. Yamakata, and K. I. Funakoshi, A first-order liquid-liquid phase transition in phosphorus, *Nature (London)* **403**, 170 (2000).
- [19] Y. Katayama, Y. Inamura, T. Mizutani, M. Yamakata, W. Utsumi, and O. Shimomura, Macroscopic separation of dense fluid phase and liquid phase of phosphorus, *Science* **306**, 848 (2004).
- [20] G. Monaco, S. Falconi, W. A. Crichton, and M. Mezouar, Nature of the First-Order Phase Transition in Fluid Phosphorus at High Temperature and Pressure, *Phys. Rev. Lett.* **90**, 255701 (2003).
- [21] T. Morishita, Liquid-Liquid Phase Transitions of Phosphorus via Constant-Pressure First-Principles Molecular Dynamics Simulations, *Phys. Rev. Lett.* **87**, 105701 (2001).
- [22] Y. Senda, F. Shimojo, and K. Hoshino, The metal-nonmetal transition of liquid phosphorus by ab initio molecular-dynamics simulations, *J. Phys. Condens. Matter* **14**, 3715 (2002).
- [23] P. Ballone and R. Jones, A reactive force field simulation of liquid-liquid phase transitions in phosphorus, *J. Chem. Phys.* **121**, 8147 (2004).
- [24] L. M. Ghiringhelli and E. J. Meijer, Phosphorus: First principle simulation of a liquid-liquid phase transition, *J. Chem. Phys.* **122**, 184510 (2005).
- [25] L. M. Ghiringhelli and E. J. Meijer, Simulating the phosphorus fluid-liquid phase transition up to the critical point, *J. Phys. Condens. Matter* **19**, 416104 (2007).
- [26] G. Zhao, H. Wang, D. Hu, M. Ding, X. Zhao, and J. Yan, Anomalous phase behavior of first-order fluid-liquid phase transition in phosphorus, *J. Chem. Phys.* **147**, 204501 (2017).
- [27] J. Behler and M. Parrinello, Generalized Neural-Network Representation of High-Dimensional Potential-Energy Surfaces, *Phys. Rev. Lett.* **98**, 146401 (2007).
- [28] J. Behler, Perspective: Machine learning potentials for atomistic simulations, *J. Chem. Phys.* **145**, 170901 (2016).
- [29] J. Behler, Neural network potential-energy surfaces in chemistry: A tool for large-scale simulations, *Phys. Chem. Chem. Phys.* **13**, 17930 (2011).
- [30] K. Yao, J. E. Herr, D. W. Toth, R. Mckintyre, and J. Parkhill, The tensormol-0.1 model chemistry: A neural network augmented with long-range physics, *Chem. Sci.* **9**, 2261 (2018).
- [31] J. Behler, First principles neural network potentials for reactive simulations of large molecular and condensed systems, *Angew. Chem., Int. Ed. Engl.* **56**, 12828 (2017).
- [32] B. Cheng, G. Mazzola, C. J. Pickard, and M. Ceriotti, Evidence for supercritical behaviour of high-pressure liquid hydrogen, *Nature (London)* **585**, 217 (2020).
- [33] J. S. Smith, O. Isayev, and A. E. Roitberg, Ani-1: An extensible neural network potential with dft accuracy at force field computational cost, *Chem. Sci.* **8**, 3192 (2017).
- [34] L. Shen, J. Wu, and W. Yang, Multiscale quantum mechanics/molecular mechanics simulations with neural networks, *J. Chem. Theory Comput.* **12**, 4934 (2016).
- [35] L. Shen and W. Yang, Molecular dynamics simulations with quantum mechanics/molecular mechanics and adaptive neural networks, *J. Chem. Theory Comput.* **14**, 1442 (2018).
- [36] L. Bonati and M. Parrinello, Silicon Liquid Structure and Crystal Nucleation from ab initio Deep Metadynamics, *Phys. Rev. Lett.* **121**, 265701 (2018).
- [37] H. Niu, L. Bonati, P. M. Piaggi, and M. Parrinello, Ab-initio phase diagram and nucleation of gallium, *Nat. Commun.* **11**, 1 (2020).
- [38] M. Yang, L. Bonati, D. Polino, and M. Parrinello, Using metadynamics to build neural network potentials for reactive events: The case of urea decomposition in water, *Catal. Today* (2021), <https://doi.org/10.1016/j.cattod.2021.03.018>.
- [39] L. Zhang, J. Han, H. Wang, R. Car, and E. Weinan, Deep Potential Molecular Dynamics: A Scalable Model with the Accuracy of Quantum Mechanics, *Phys. Rev. Lett.* **120**, 143001 (2018).
- [40] L. Zhang, J. Han, H. Wang, W. A. Saidi, R. Car, and E. Weinan, End-to-end symmetry preserving inter-atomic potential energy model for finite and extended systems, in *Proceedings of the 32nd International Conference on Neural Information Processing Systems, NIPS'18* (Curran Associates Inc., Red Hook, 2018), p. 4441–4451, <https://dl.acm.org/doi/10.5555/3327345.3327356>.
- [41] V. L. Deringer, M. A. Caro, and G. Csányi, A general-purpose machine-learning force field for bulk and nanostructured phosphorus, *Nat. Commun.* **11**, 5461 (2020).
- [42] P. M. Piaggi and M. Parrinello, Multithermal-Multibaric Molecular Simulations from a Variational Principle, *Phys. Rev. Lett.* **122**, 050601 (2019).
- [43] P. M. Piaggi and M. Parrinello, Calculation of phase diagrams in the multithermal-multibaric ensemble, *J. Chem. Phys.* **150**, 244119 (2019).
- [44] See Supplemental Material, which includes Refs. [45–60], at <http://link.aps.org/supplemental/10.1103/PhysRevLett.127.080603> for details about the computational setup used, the implementation of the NN training and validation, and additional results.
- [45] S. Maintz, V. L. Deringer, A. L. Tchougréeff, and R. Dronskowski, LOBSTER: A tool to extract chemical bonding from plane-wave based DFT, *J. Comput. Chem.* **37**, 1030 (2016).
- [46] J. P. Perdew, K. Burke, and M. Ernzerhof, Generalized Gradient Approximation Made Simple, *Phys. Rev. Lett.* **77**, 3865 (1996).
- [47] S. Goedecker, M. Teter, and J. Hutter, Separable dual-space gaussian pseudopotentials, *Phys. Rev. B* **54**, 1703 (1996).
- [48] C. Hartwigsen, S. Goedecker, and J. Hutter, Relativistic separable dual-space gaussian pseudopotentials from h to RN, *Phys. Rev. B* **58**, 3641 (1998).

- [49] D. J. Evans and B. L. Holian, The nose–hoover thermostat, *J. Chem. Phys.* **83**, 4069 (1985).
- [50] S. Melchionna, G. Ciccotti, and B. Lee Holian, Hoover NPT dynamics for systems varying in shape and size, *Mol. Phys.* **78**, 533 (1993).
- [51] J. Sun, A. Ruzsinszky, and J. P. Perdew, Strongly Constrained and Appropriately Normed Semilocal Density Functional, *Phys. Rev. Lett.* **115**, 036402 (2015).
- [52] S. Grimme, S. Ehrlich, and L. Goerigk, Effect of the damping function in dispersion corrected density functional theory, *J. Comput. Chem.* **32**, 1456 (2011).
- [53] S. Plimpton, Fast parallel algorithms for short-range molecular dynamics, *J. Comput. Phys.* **117**, 1 (1995).
- [54] G. A. Tribello, M. Bonomi, D. Branduardi, C. Camilloni, and G. Bussi, Plumed 2: New feathers for an old bird, *Comput. Phys. Commun.* **185**, 604 (2014).
- [55] M. Parrinello and A. Rahman, Polymorphic transitions in single crystals: A new molecular dynamics method, *J. Appl. Phys.* **52**, 7182 (1981).
- [56] H. Wang, L. Zhang, J. Han, and E. Weinan, Deepmd-kit: A deep learning package for many-body potential energy representation and molecular dynamics, *Comput. Phys. Commun.* **228**, 178 (2018).
- [57] V. L. Deringer, N. Bernstein, G. Csányi, C. B. Mahmoud, M. Ceriotti, M. Wilson, D. A. Drabold, and S. R. Elliott, Origins of structural and electronic transitions in disordered silicon, *Nature (London)* **589**, 59 (2021).
- [58] P. Giannozzi *et al.*, Quantum espresso: A modular and open-source software project for quantum simulations of materials, *J. Phys. Condens. Matter* **21**, 395502 (2009).
- [59] P. Giannozzi *et al.*, Advanced capabilities for materials modelling with quantum espresso, *J. Phys. Condens. Matter* **29**, 465901 (2017).
- [60] P. Giannozzi, O. Baseggio, P. Bonf, D. Brunato, R. Car, I. Carnimeo, C. Cavazzoni, S. de Gironcoli, P. Delugas, F. Ferrari Ruffino, A. Ferretti, N. Marzari, I. Timrov, A. Urru, and S. Baroni, Quantum espresso toward the exascale, *J. Chem. Phys.* **152**, 154105 (2020).
- [61] P. M. Piaggi and M. Parrinello, Multithermal-Multibaric Molecular Simulations from a Variational Principle, *Phys. Rev. Lett.* **122**, 050601 (2019).
- [62] M. Invernizzi, P. M. Piaggi, and M. Parrinello, Unified Approach to Enhanced Sampling, *Phys. Rev. X* **10**, 041034 (2020).
- [63] A. Laio and M. Parrinello, Escaping free-energy minima, *Proc. Natl. Acad. Sci. U.S.A.* **99**, 12562 (2002).
- [64] A. Barducci, G. Bussi, and M. Parrinello, Well-Tempered Metadynamics: A Smoothly Converging and Tunable Free-Energy Method, *Phys. Rev. Lett.* **100**, 020603 (2008).
- [65] O. Valsson, P. Tiwary, and M. Parrinello, Enhancing important fluctuations: Rare events and metadynamics from a conceptual viewpoint, *Annu. Rev. Phys. Chem.* **67**, 159 (2016).
- [66] M. Invernizzi and M. Parrinello, Rethinking metadynamics: From bias potentials to probability distributions, *J. Phys. Chem. Lett.* **11**, 2731 (2020).
- [67] H. Niu, P. M. Piaggi, M. Invernizzi, and M. Parrinello, Molecular dynamics simulations of liquid silica crystallization, *Proc. Natl. Acad. Sci. U.S.A.* **115**, 5348 (2018).
- [68] L. Zhang, D.-Y. Lin, H. Wang, R. Car, and E. Weinan, Active learning of uniformly accurate interatomic potentials for materials simulation, *Phys. Rev. Mater.* **3**, 023804 (2019).
- [69] Y. Zhang, H. Wang, W. Chen, J. Zeng, L. Zhang, H. Wang, and E. Weinan, DP-GEN: A concurrent learning platform for the generation of reliable deep learning based potential energy models, *Comput. Phys. Commun.* **253**, 107206 (2020).
- [70] K. Binder, Critical Properties from Monte Carlo Coarse Graining and Renormalization, *Phys. Rev. Lett.* **47**, 693 (1981).
- [71] H. Watanabe, N. Ito, and C.-K. Hu, Phase diagram and universality of the Lennard-Jones gas-liquid system, *J. Chem. Phys.* **136**, 204102 (2012).